

Supporting Information

Unlocking the Sensing Potential of Phenyl-Substituted Perylene Diimides Under Extreme Conditions

Paulina Ratajczyk,^a Szymon Sobczak,^{a*} Przemysław Woźny,^a Angelika Wcisło,^a Tomasz Poręba,^b Andrzej Katrusiak^{a*}

^a Faculty of Chemistry, Adam Mickiewicz University, Uniwersytetu Poznańskiego 8, 61-614 Poznań, Poland

^b European Synchrotron Radiation Facility, 71 Avenue des Martyrs, 38000 Grenoble, France

*e-mail: szymon.sobczak@amu.edu.pl; katran@amu.edu.pl

1. *N,N'-diphenyl-3,4,9,10-perylenedicarboximide recrystallization*

10 mg of *N,N'*-Diphenyl-3,4,9,10-perylenedicarboximide has been placed at the bottom of the glass capillary (\varnothing 5 mm); the capillary has been fine-scaled and the bottom of the capillary has been heated with a heat-gun to 400 °C. The pink plate-like crystals started growing around 1 mm above the level of the crude product.

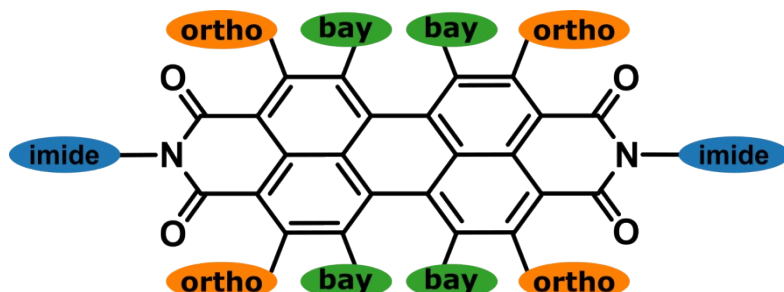


Figure S1. Chemical structure of a PDI showing the different positions for substitutions: imide, ortho and bay positions.

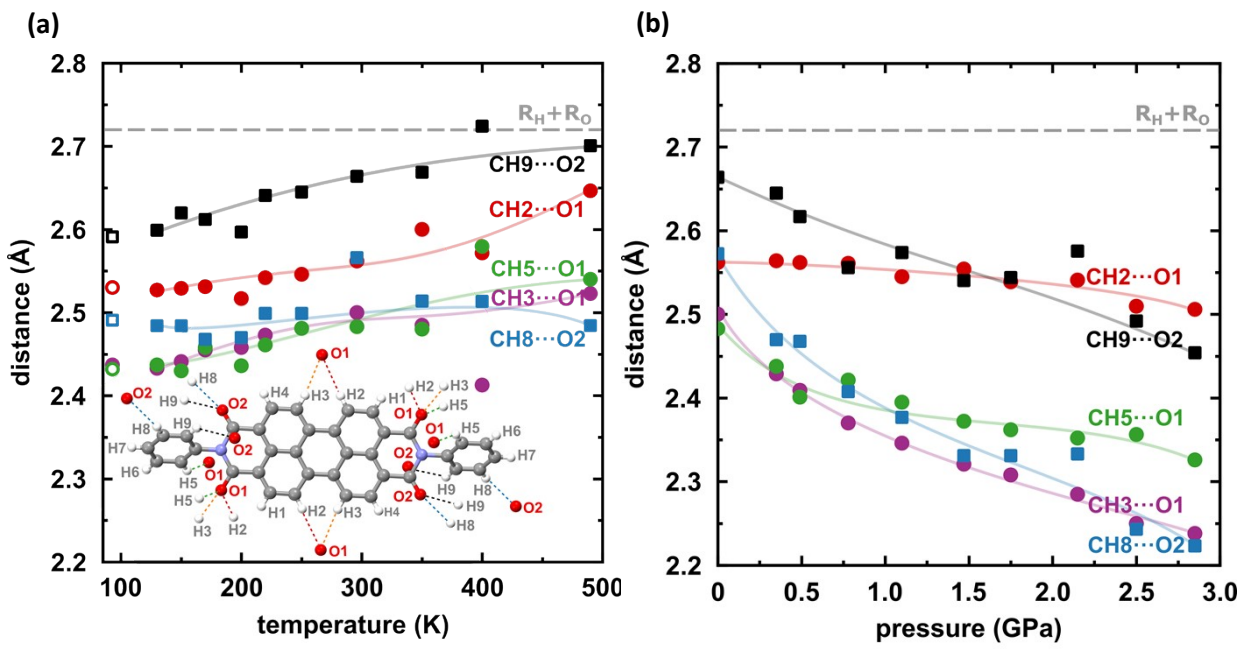


Figure S2. Closest $\text{CH}\cdots\text{O}$ contacts plotted as a function of (a) temperature, and (b) pressure in the structure of PTCDI-Ph phase II. Open symbols refer to the interactions at 93 K in the structure reported by Sato and Mizuguchi.¹ The horizontal dashed lines indicate the sums of van der Waals radii.²

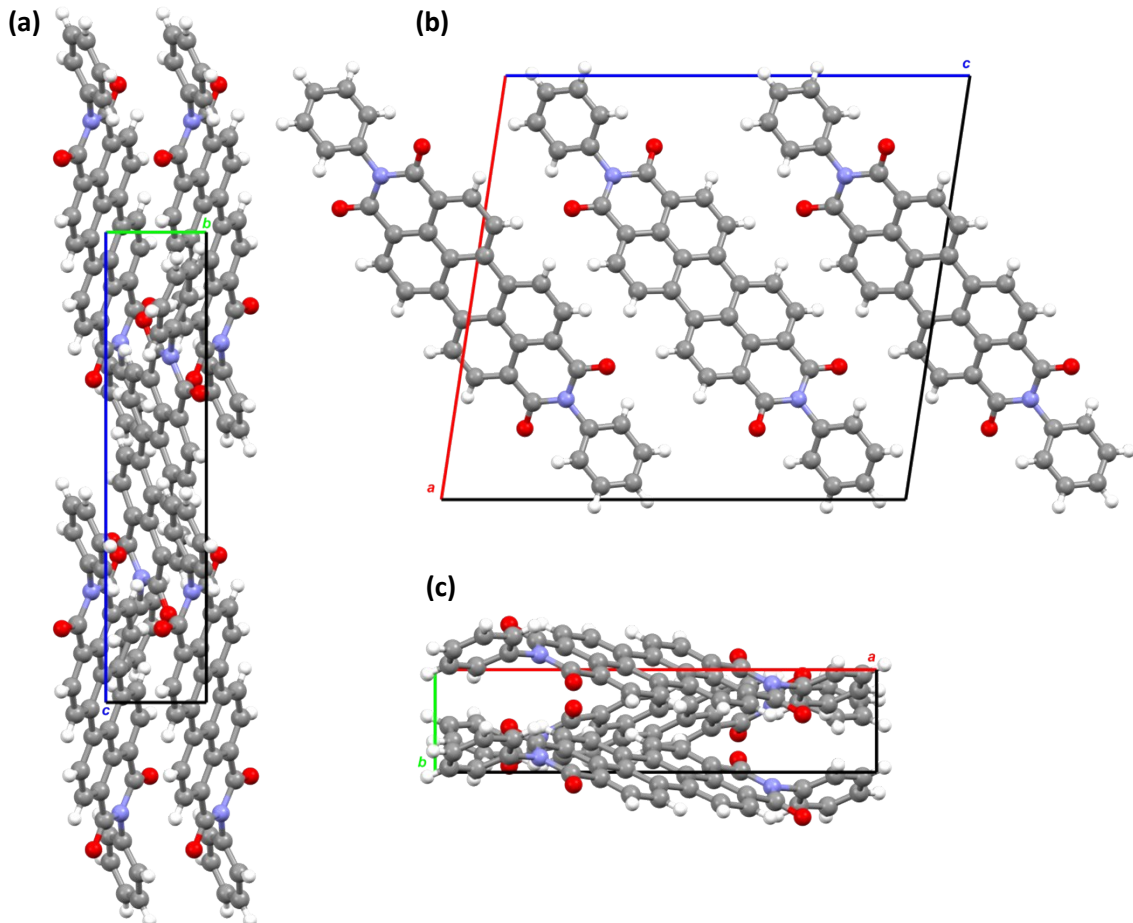


Figure S3. Arrangements of PTCDI-Ph molecules in the unit-cell along direction: (a) [100]; (b) [010]; and (c) [001], at 0.348 GPa.

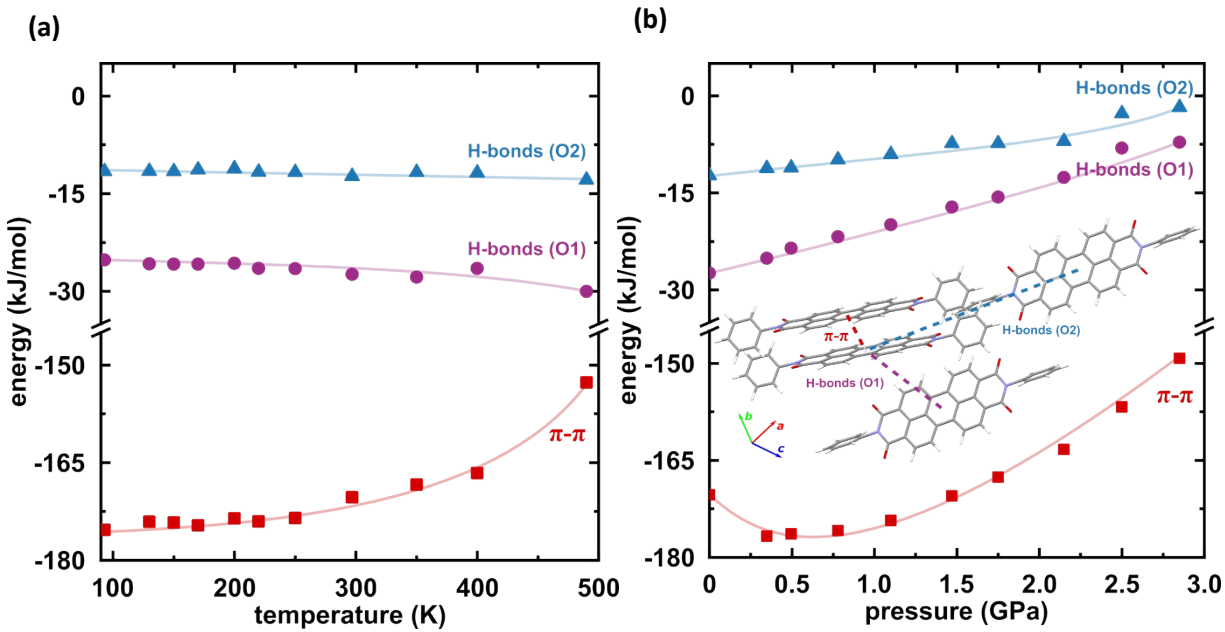


Figure S4. Intermolecular potentials as a function of temperature (a) and pressure (b) calculated for adjacent molecules, as shown in the inset of Figure b. The calculations show the energy change in the intermolecular interactions. The H-atom sites were normalized for the H-bond lengths. Inter-molecular potentials were calculated using the ‘UNI’ force field.^{3,4}

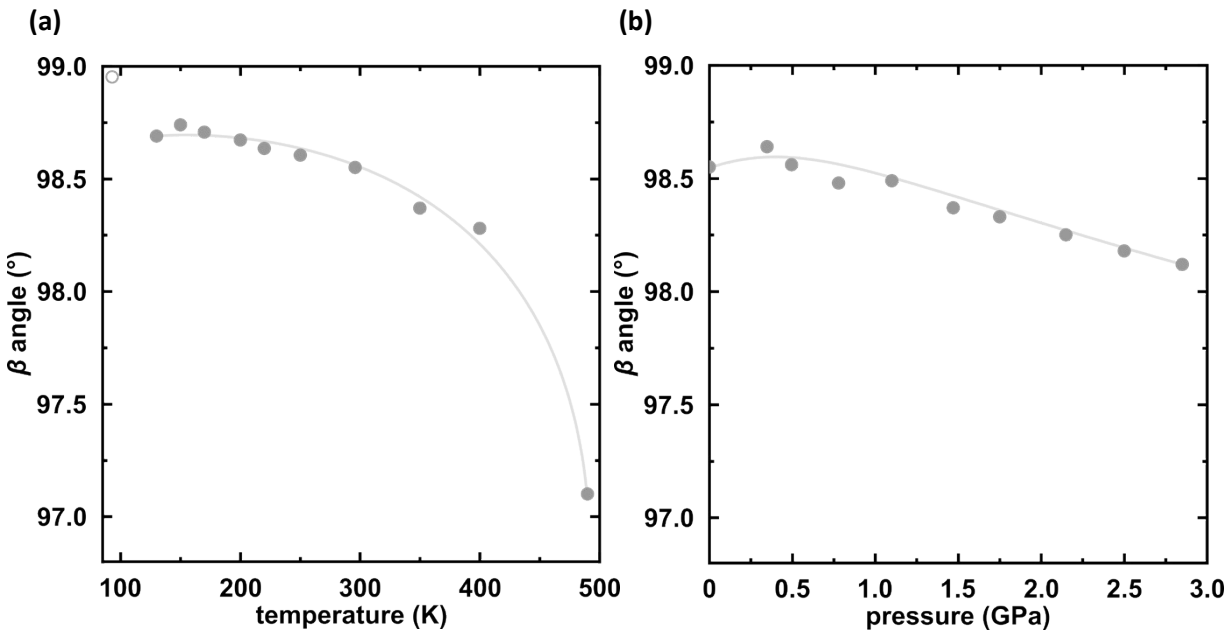


Figure S5. Temperature (a) and pressure (b) dependence of the β angle for the PTCDI-Ph crystal phase II. Open symbol refers to the previously reported structure by Sato and Mizuguchi.¹ The estimated standard deviations (ESDs) are smaller than the symbols.

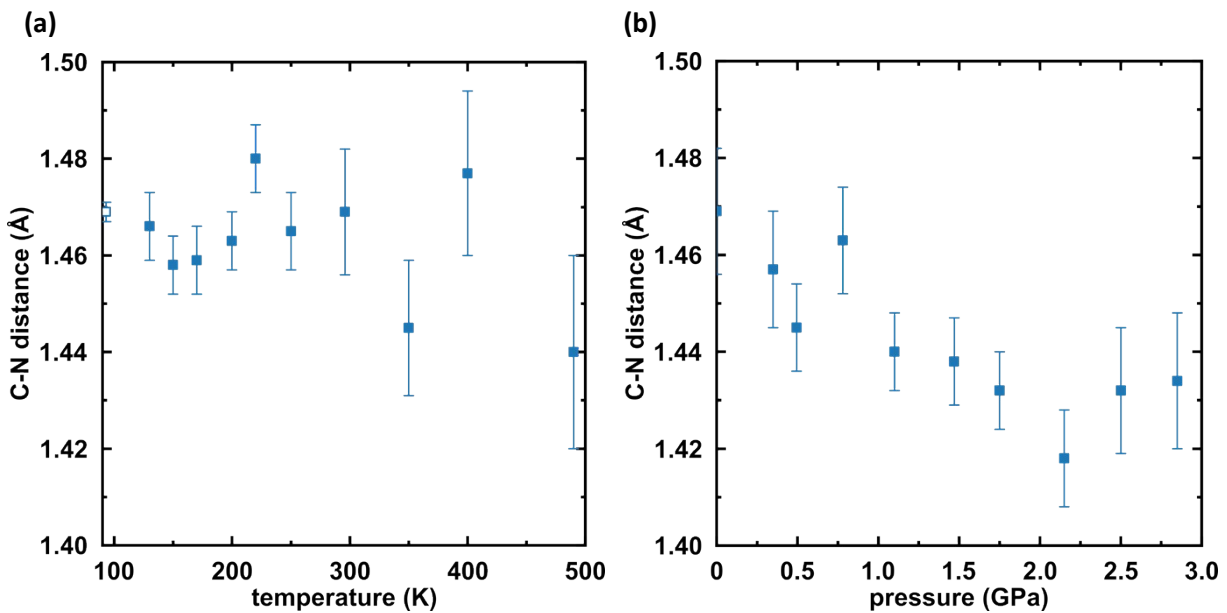


Figure S6. Bond distance N1-C13 as a function of temperature (a) and pressure (b). The open symbol refers to the previously reported structure by Sato and Mizuguchi.¹

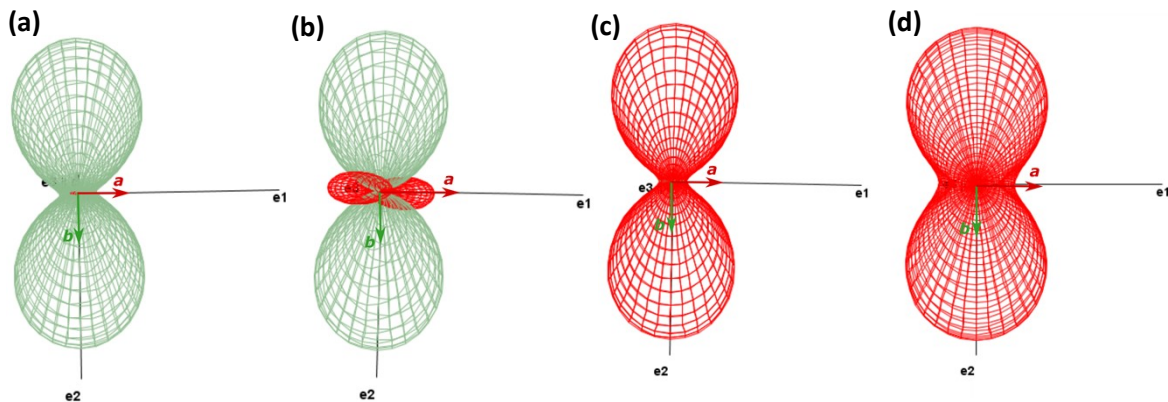


Figure S7. Graphical representations of the tensors of thermal expansion in the range of 130 – 250 K (a) and 300 – 490 K (b), and compressibility in the range of 0.1 MPa – 0.78 GPa (c), and 1.10 – 2.85 GPa for the PTCDI-Ph crystal, calculated by program TEV (Thermal Expansion Visualizing).⁵

Table S1. Linear coefficients of thermal expansion of PTCDI-Ph in the range of 130 – 250 K.

Axes	$\alpha(\text{MK}^{-1})$	$\sigma\alpha(\text{MK}^{-1})$	Direction		
			a	b	c
X_1	-2.0800	3.7078	0.9807	-0.0000	-0.1956
X_2	10.8157	4.0129	0.3631	-0.0000	0.9318
X_3	83.5214	16.6352	0.0000	-1.0000	0.0000
V	97.3355	9.6480			

Table S2. Linear coefficients of thermal expansion of PTCDI-Ph in the range of 300 – 490 K.

Axes	$\alpha(\text{MK}^{-1})$	$\sigma\alpha(\text{MK}^{-1})$	Direction		
			<i>a</i>	<i>b</i>	<i>c</i>
\mathbf{X}_1	-200.5138	22.1898	-0.4993	0.0000	0.8664
\mathbf{X}_2	5.4518	3.8478	-0.8688	0.0000	-0.4952
\mathbf{X}_3	426.5579	32.7141	-0.0000	-1.0000	0.0000
\mathbf{V}	225.4399	13.1263			

Table S3. Compressibility related to crystallographic axes calculated for PTCDI-Ph in the range of 0.1 MPa – 2.85 GPa with Birch-Murnaghan Coefficients.

Axes	$K(\text{MPa}^{-1})$	$\sigma K(\text{MPa}^{-1})$	Direction			Empirical parameters			
			<i>a</i>	<i>b</i>	<i>c</i>	ε_0	λ	P_c	v
\mathbf{X}_1	25.4079	0.9382	-0.0000	1.0000	-0.0000	8.2668e-02	-1.5756e-01	-0.0759	0.2529
\mathbf{X}_2	10.7667	0.5204	0.0134	-0.0000	0.9999	-2.1586e-04	-1.8289e-02	0.0001	0.6973
\mathbf{X}_3	3.0206	1.6691	0.9923	-0.0000	0.1236	2.9939e-03	-6.3660e-04	0.0001	2.2967
\mathbf{V}	54.2560	6.5178							

Birch-Murnaghan Coefficients

	$B_0(\text{GPa})$	$\sigma B_0(\text{GPa})$	$V_0(\text{\AA}^3)$	$\sigma V_0(\text{\AA}^3)$	B'	$\sigma B'$	$P_c(\text{GPa})$
2^{nd}	12.9080	0.8756	1193.6458	7.1626	4	n/a	0
3^{rd}	6.5913	1.7563	1211.7916	10.1746	13.2561	3.9558	0
$3^{\text{rd}} \text{ with } P_c$	6.5913	1.8970	1211.7916	10.9898	13.2561	4.2728	0

Table S4. Compressibility related to crystallographic axes calculated for PTCDI-Ph in the range of 0.1 MPa – 0.78 GPa with Birch-Murnaghan Coefficients.

Axes	$K(\text{TPa}^{-1})$	$\sigma K(\text{TPa}^{-1})$	Direction			Empirical parameters			
			<i>a</i>	<i>b</i>	<i>c</i>	ε_0	λ	P_c	v
\mathbf{X}_1	48.0177	0.0000	-0.0000	1.0000	-0.0000	3.9954e+01	-4.0024e+01	-0.2358	0.0012
\mathbf{X}_2	14.9559	0.0000	0.0873	-0.0000	0.9962	-6.1622e-05	-1.9302e-02	0.0001	0.7233
\mathbf{X}_3	-6.1215	0.0000	0.9980	-0.0000	0.0634	1.8352e-04	6.5413e-03	0.0001	0.9166
\mathbf{V}	108.7516	10.8976							

Birch-Murnaghan Coefficients

	$B_0(\text{GPa})$	$\sigma B_0(\text{GPa})$	$V_0(\text{\AA}^3)$	$\sigma V_0(\text{\AA}^3)$	B'	$\sigma B'$	$P_c(\text{GPa})$
2^{nd}	7.7532	1.1262	1214.9247	9.2233	4	n/a	0
3^{rd}	3.2471	2.6520	1220.4092	12.8058	36.5625	36.6371	0
$3^{\text{rd}} \text{ with } P_c$	7.8657	0.0000	1178.7576	0.0000	18.8242	0.0000	0.1900

Table S5. Compressibility related to crystallographic axes calculated for PTCDI-Ph in the range of 1.10 GPa – 2.85 GPa with Birch-Murnaghan Coefficients.

Axes	K(TPa ⁻¹)	σK (TPa ⁻¹)	Direction			Empirical parameters			
			a	b	c	ε_0	λ	P_c	v
X ₁	24.4550	2.2308	0.0000	-1.0000	0.0000	1.5628e+00	-1.4512e+00	-1.9036	0.0672
X ₂	10.7563	2.4226	-0.2265	-0.0000	0.9740	6.5253e-01	-5.3532e-01	-4.5691	0.1137
X ₃	3.2853	2.5547	-0.9500	0.0000	-0.3121	3.2926e-01	-3.1623e-01	-1.5221	0.0395
V	41.8901	1.9348							

Birch-Murnaghan Coefficients

	B ₀ (GPa)	σB_0 (GPa)	V ₀ (Å ³)	σV_0 (Å ³)	B'	$\sigma B'$	P _c (GPa)
2 nd	15.6498	1.0297	1173.1416	6.8336	4	n/a	0
3 rd	15.0724	10.4216	1175.0773	36.3956	4.3219	5.8827	0
3 rd with P _c	15.8886	11.4223	1160.7406	32.9795	4.2704	7.0264	0.1900

Table S6. Pitch and roll angles and interlayer distance at high pressure.

Pressure	Pitch angle (°)	Roll angle (°)	d _{π-π} (Å)
0.1 MPa	6.18	28.15	3.523
0.35 GPa	5.57	26.69	3.421
0.49 GPa	5.37	26.27	3.389
0.78 GPa	5.15	25.87	3.352
1.1 GPa	4.91	25.73	3.320
1.47 GPa	4.72	25.48	3.287
1.75 GPa	4.55	25.41	3.262
2.15 GPa	4.29	25.21	3.235
2.50 GPa	4.10	25.18	3.203
2.85 GPa	3.97	25.18	3.183

Table S7. Pitch and roll angles and interlayer distance at various temperatures.

Temperature (K)	Pitch angle (°)	Roll angle (°)	d _{π-π} (Å)
93	6.08	26.55	3.449
130	6.14	27.08	3.472
150	6.13	27.07	3.475
170	6.10	26.98	3.480
200	6.07	27.09	3.478
220	6.03	27.51	3.480
250	6.13	27.44	3.498
296	6.18	28.15	3.523
350	6.39	29.25	3.539
400	6.06	29.22	3.560
490	6.71	34.13	3.592

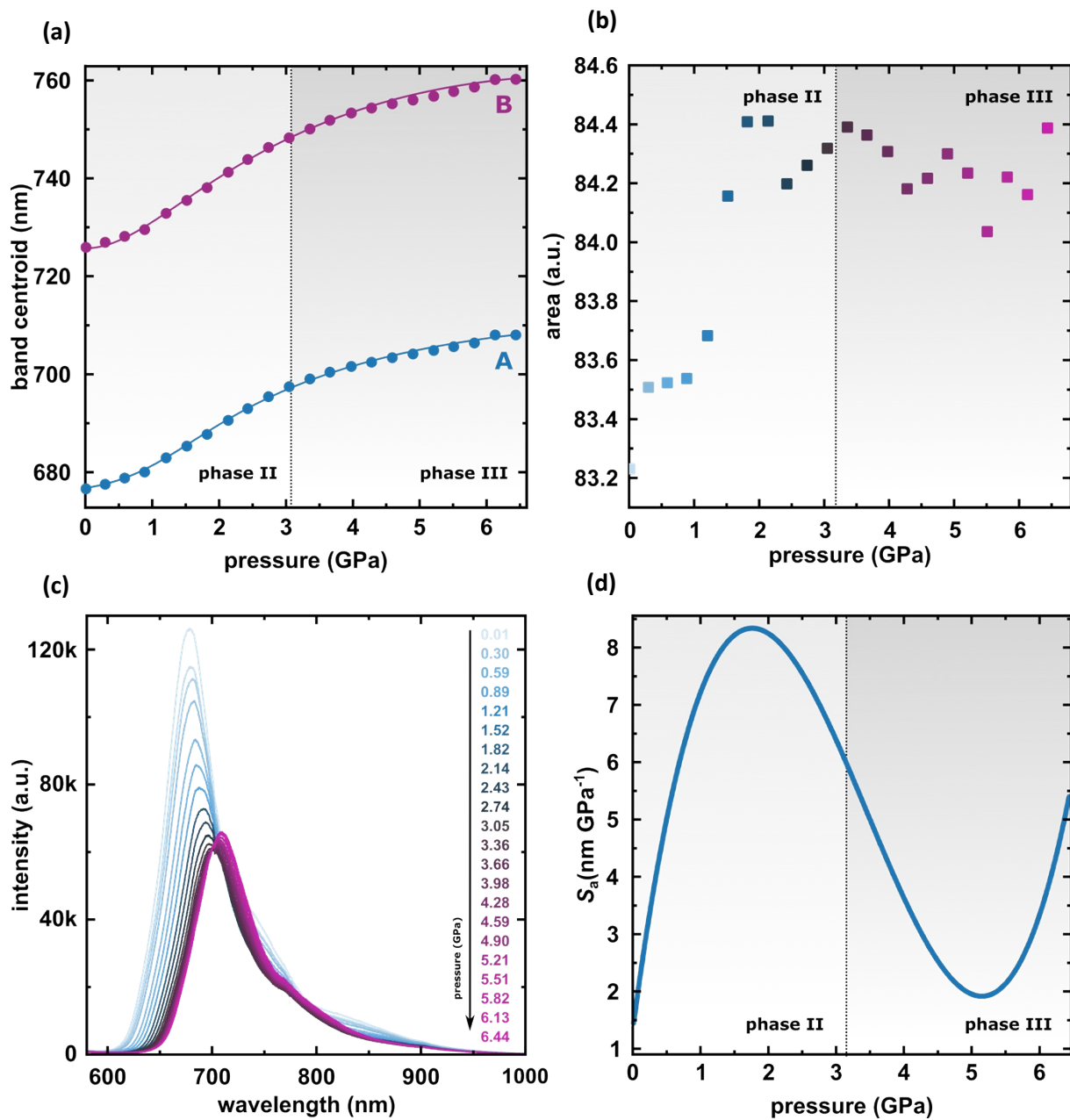


Figure S8. Band centroids shifts (a), changes of the emission bands area (b), emission spectra of the PTCDI-Ph recorded in compression cycle up to 6.44 GPa (c), and changes of absolute sensitivity (d) in high-pressure conditions.

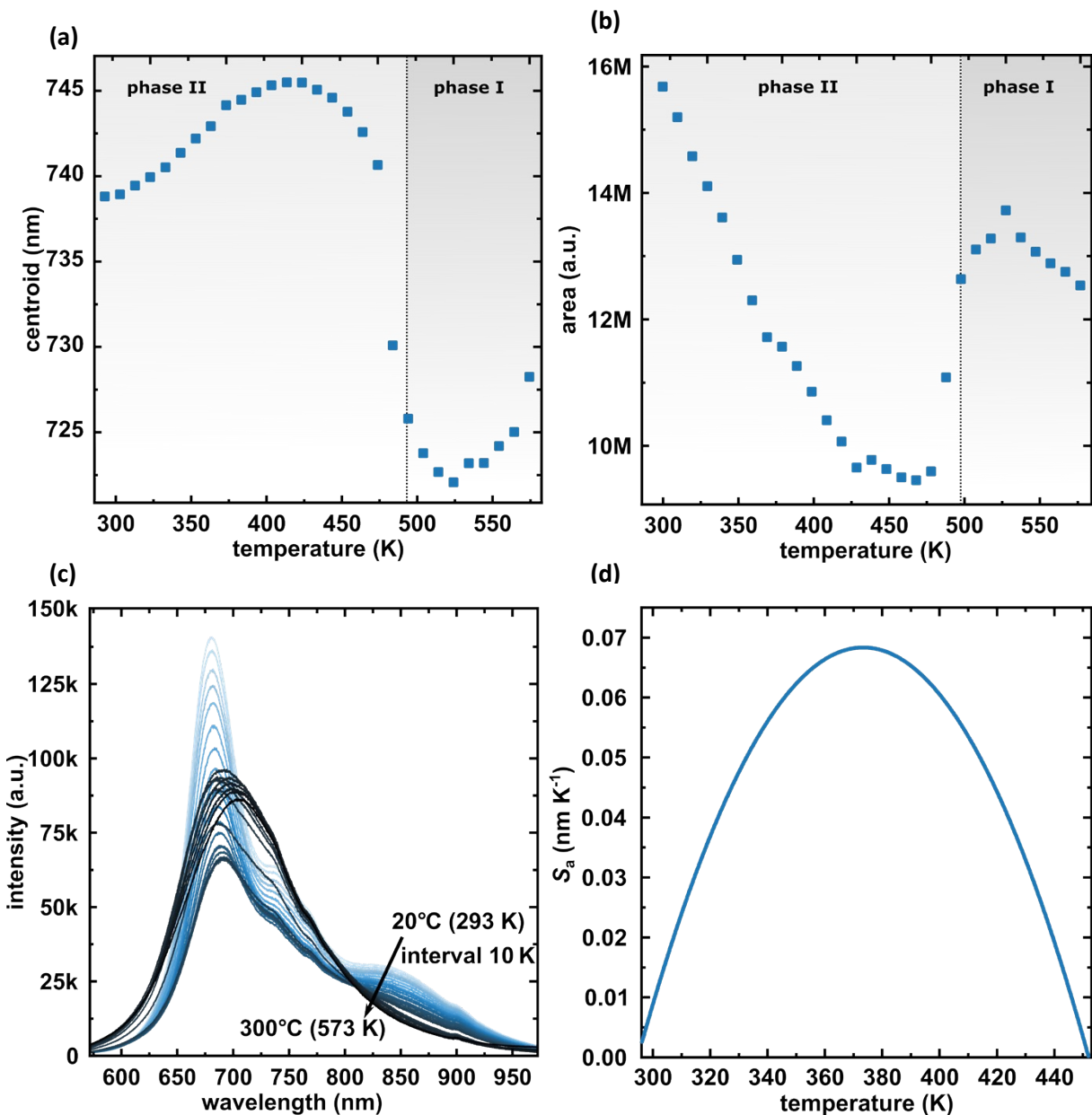


Figure S9. Changes of the emission bands centroid (a), and area (b) as a function of temperature. Emission spectra of the PTCDI-Ph recorded in temperature range from 293 K to 573 K (c). Changes of absolute sensitivity (d) in high-temperature conditions.

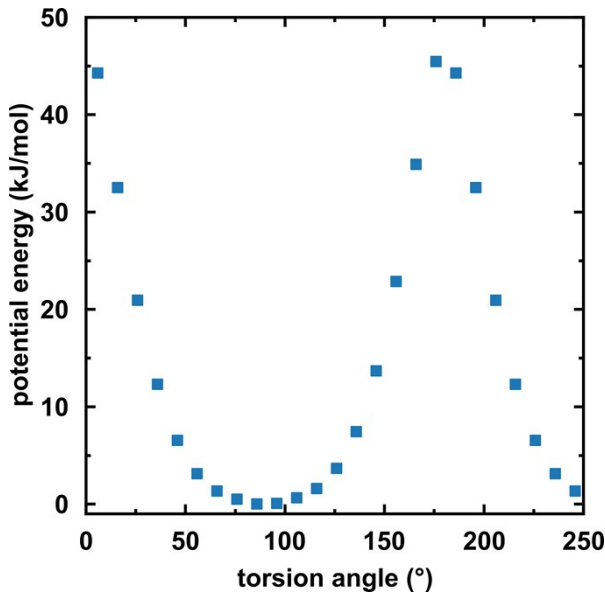


Figure S10. Potential energy of the isolated PTCI-Ph molecule with rotation around one torsion angle (another τ was fixed at 55.92° as derived from the X-ray measurement).

Fitting of band shift in high-pressure conditions:

4-order polynomial function for the shift in the high pressure conditions was presented below:

$$y = A_0 + A_1P^1 + A_2P^2 + A_3P^3 + A_4P^4,$$

where A_0, A_1, A_2, A_3 , and A_4 are constant, and P are measured parameter (pressure).

For the shift of the emission band at = 676 nm in pressure the constant values were:

$$A_0 = 676.52 \pm 0.28, A_1 = 1.33 \pm 0.63, A_2 = 4.49 \pm 0.41, A_3 = -1.14 \pm 0.097, \text{ and } A_4 = 0.083 \pm 0.007.$$

Fitting of band shift in high-temperature conditions:

4-order polynomial function for the shift in the high temperature conditions was presented below:

$$y = B_0 + B_1T^1 + B_2T^2 + B_3T^3 + B_4T^4,$$

where B_0, B_1, B_2, B_3 , and B_4 are constant, and T are measured parameter (temperature in K).

For the shift of the emission band at = 676 nm in pressure the constant values were:

$$B_0 = 1133.99 \pm 107.33, B_1 = -3.83 \pm 1.15, B_2 = 0.013 \pm 0.005, B_3 = -1.75 \times 10^{-5} \pm 8.00 \times 10^{-6}, \text{ and } B_4 = 7.41 \times 10^{-9} \pm 5.22 \times 10^{-9}.$$

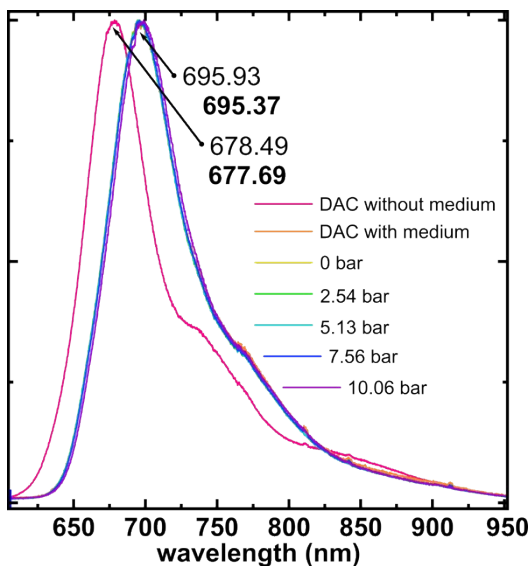


Figure S11. Comparison of the spectrum from the DAC chamber with and without the medium. The bold values are the result of deconvolution.

Table S8. Comparison of the most sensitive, shift-based sensors under extreme conditions of pressure and temperature.

Host/Emitting ion	Sensitivity line shift		λ (nm)	References
	nm K^{-1}	nm GPa^{-1}		
PTCDI-Ph	6.8×10^{-2}	6.26	680	This work
YVO ₄ /Er ³⁺	-5.16×10^{-3}	1.766	1605	6
SrFCI/ Sm ²⁺	-2.3×10^{-3}	1.11	690	7
BaLi ₂ Al ₂ Si ₂ N ₆ / Eu ²⁺	—	1.58	532	8
Y ₂ SiO ₅ / Pr ³⁺	—	1.04	320	9
Y ₂ Ge _{0.10} Si _{0.90} O ₅ / Pr ³⁺	—	1.28	320	9
YAlO ₃ / Cr ³⁺	7.6×10^{-3}	0.7	723	10
NaBiF ₄ / Er ³⁺	—	-0.8	1503	11
Bi ₂ MoO ₆ / Er ³⁺ , Tm ³⁺ , Yb ³⁺	8.5×10^{-3}	—	700/670	12
SrB ₄ O ₇ / Eu ²⁺	4.8×10^{-4}	0.17	362.7	13
LaPO ₄ /Tm ³⁺	-2×10^{-3}	0.1	475	14
Al ₂ O ₃ /Cr ³⁺	6.2×10^{-3}	0.365		15

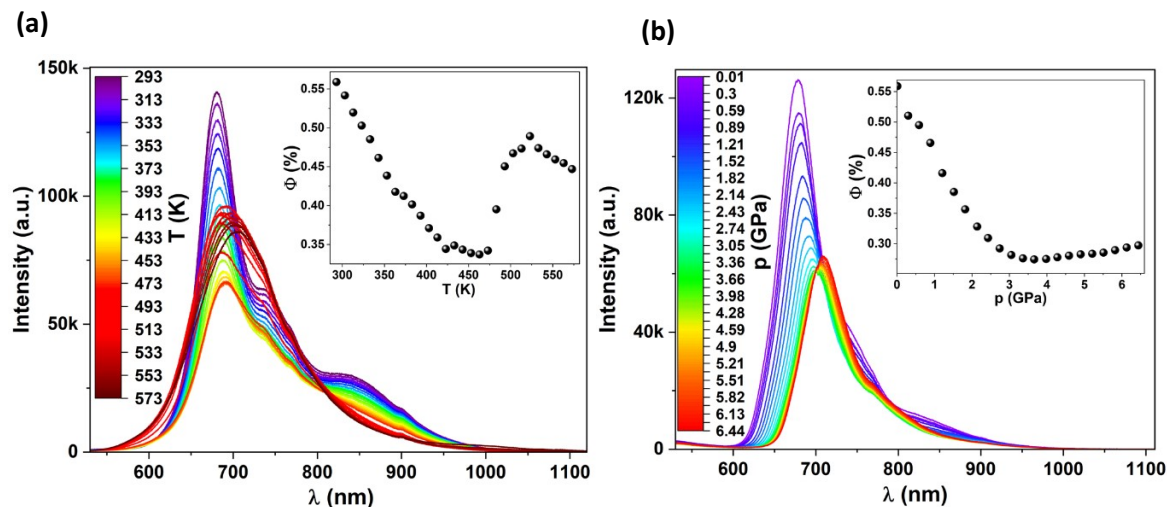


Figure S12. Luminescence intensity changes as a function of temperature (a) and pressure (b). Insets: changes of quantum yield as a function of applied conditions.

Changes in optical properties, such as luminescence colour, were previously reported as indicators of phase transitions in luminescent materials under variable physical conditions. To demonstrate the observed colour changes of the visible luminescence, we calculated chromaticity coordinates based on the recorded emission spectra under high-temperature and high-pressure conditions and prepared a CIE 1931 diagram (Fig. S11a). Gradual shifts in the luminescence colour towards the red region of the CIE diagram were observed under both high-temperature and high-pressure conditions.

Under high-temperature conditions, the points on the chromaticity diagram shift linearly from 293 K ($x \approx 0.669$, $y \approx 0.315$) to 463 K ($x \approx 0.653$, $y \approx 0.331$), with the trend changing near the phase transition from phase II to phase I (at approximately 483 K). After the phase transition, the material exhibits a more pure luminescence colour, closer to the edge of the CIE diagram. The luminescence colour continues to change linearly with increasing temperature due to the emission-band broadening.

The chromaticity coordinates for the emission spectra under high-pressure conditions also exhibit a linear trend across the entire pressure range, from 0.01 GPa ($x \approx 0.670$, $y \approx 0.315$) to 6.44 GPa ($x \approx 0.675$, $y \approx 0.310$). The transition from the phase II to the phase III is observed as a pause in the shift of chromaticity coordinates in the pressure range from 3.05 to 3.98 GPa. Further increases of pressure value in the system also influenced the visible luminescence colour change.

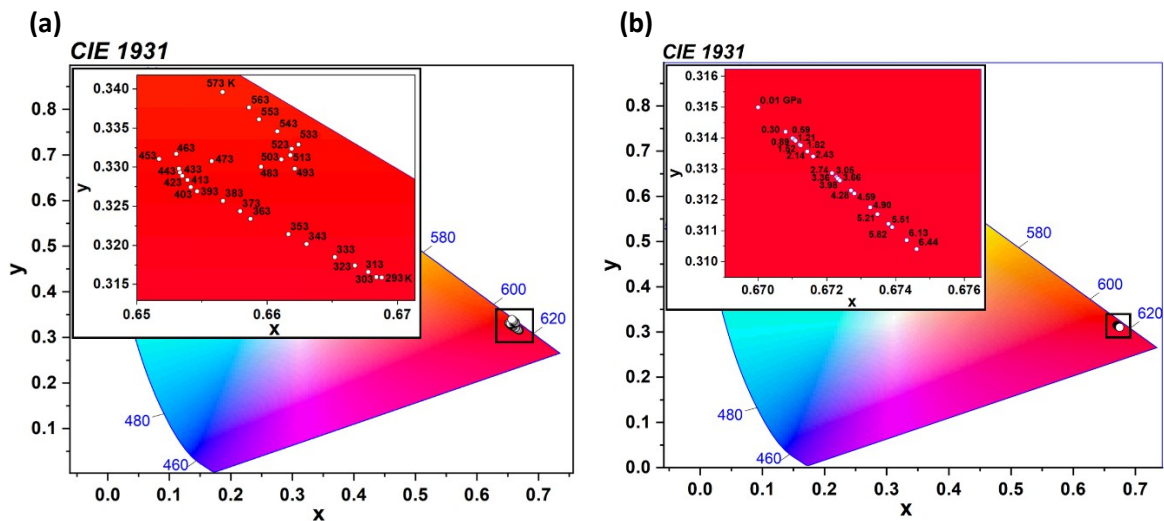


Figure S13. The CIE 1931 diagram for the PTCDI-Ph according to the applied temperature (a) and pressure (b). The insets magnify the regions roughly indicated by square frames.

Table S9. HOMO and LUMO energies for PTCDI-Ph under high-pressure conditions.

Pressure	HOMO (eV)	LUMO (eV)	ΔE (eV)
0.1 MPa	-9.404	-2.806	6.598
0.348 GPa	-9.408	-2.809	6.599
0.495 GPa	-9.411	-2.813	6.598
0.78 GPa	-9.412	-2.813	6.599
1.10 GPa	-9.412	-2.816	6.596
1.47 GPa	-9.413	-2.816	6.597
1.75 GPa	-9.413	-2.816	6.597
2.15 GPa	-9.414	-2.818	6.596
2.50 GPa	-9.415	-2.818	6.597
2.85 GPa	-9.415	-2.818	6.597

Table S10. HOMO and LUMO energies for PTCDI-Ph at various temperatures.

Temperature [K]	HOMO (eV)	LUMO (eV)	ΔE (eV)
130	-9.407	-2.808	6.599
150	-9.406	-2.808	6.598
170	-9.407	-2.810	6.597
200	-9.405	-2.807	6.598
220	-9.407	-2.808	6.599
250	-9.405	-2.806	6.599
350	-9.401	-2.804	6.597
400	-9.403	-2.805	6.598
490	-9.389	-2.789	6.600

Table S11. Detailed crystallographic data for PTCDI-Ph at low temperature.

Temperature	130 K	150 K	170 K	200 K	220 K	250 K	350 K	400 K	490 K	
CCDC numbers	2253193	2253194	2253195	2253196	2253197	2253198	2253199	2253200	2253201	
Crystal system	monoclinic									
Space group	<i>P</i> 2 ₁ /c									
<i>a</i> (Å)	16.755(5)	16.749(4)	16.755(2)	16.7559(14)	16.7581(13)	16.7456(12)	16.706(3)	16.680(10)	16.52(3)	
<i>b</i> (Å)	3.9243(13)	3.9271(12)	3.9289(7)	3.9338(3)	3.9442(4)	3.9671(3)	4.0610(6)	4.1044(13)	4.344(4)	
Unit cell dimensions	<i>c</i> (Å)	18.288(4)	18.296(4)	18.307(2)	18.3169(13)	18.3139(13)	18.3012(12)	18.291(3)	18.246(8)	17.92(4)
α (°)	90	90	90	90	90	90	90	90	90	
β (°)	98.69(2)	98.74(2)	98.707(13)	98.673(7)	98.635(7)	98.605(6)	98.37(2)	98.28(5)	97.10(19)	
γ (°)	90	90	90	90	90	90	90	90	90	
Volume (Å ³)	1188.7(6)	1189.4(5)	1191.2(3)	1193.53(17)	1196.78(17)	1202.09(15)	1227.7(3)	1236.1(10)	1276(4)	
Z/Z'	2/0.5	2/0.5	2/0.5	2/0.5	2/0.5	2/0.5	2/0.5	2/0.5	2/0.5	
Calculated density (g/cm ³)	1.516	1.515	1.513	1.510	1.506	1.499	1.468	1.458	1.425	
Absorption (mm ⁻¹)	0.809	0.809	0.808	0.806	0.804	0.800	0.784	0.778	0.761	
F(000)	560.0	560.0	560.0	560.0	560.0	560.0	560.0	560.0	560.0	
Crystal size (mm)	0.13x0.04x0.02									
2θ-range for data collection (°)	5.336 to 147.808	5.338 to 147.19	5.336 to 147.802	5.336 to 147.32	5.334 to 146.762	5.338 to 147.32	5.346 to 141.978	10.72 to 142.302	9.946 to 100.768	
Min/max indices: h, k, l	-20/20,-4/3,- 20/22	-20/20,-4/3,- 21/22	-20/20,-4/3,- 21/22	-20/20,-4/3,- 21/22	-20/20,-4/3,- 21/22	-20/20,-4/3,- 20/22	-20/18,-4/1,- 21/16	-18/20,-4/1,- 16/21	-15/15,-4/2,- 17/17	
Reflect. Collected/unique	4469/2316	4510/2320	4514/2323	4589/2331	4605/2333	4607/2339	3988/2217	3887/2202	2798/1129	
Data/restrains/parameters	2316/0/191	2320/0/191	2323/0/191	2331/0/191	2333/0/191	2339/0/191	2217/177/201	2202/177/201	1129/84/42	
Goodness-of-fit on F2	0.942	0.912	0.918	0.904	0.934	0.959	0.725	0.743	0.637	
Final R1/wR2 (I>2σ1)	0.0901/0.1651	0.0804/0.1445	0.0856/0.1481	0.0877/0.1387	0.0857/0.1513	0.0943/0.1848	0.1163/0.1053	0.0932/0.0911	0.0772/0.1370	
R1/wR2 (all data)	0.2234/0.2476	0.2150/0.2340	0.2255/0.2366	0.2232/0.2204	0.2166/0.2340	0.2493/0.2849	0.5547/0.2309	0.5712/0.2223	0.6674/0.3347	
Largest diff. peak/hole (e.Å ⁻³)	0.33/-0.38	0.28/-0.33	0.27/-0.33	0.30/-0.31	0.31/-0.34	0.30/-0.33	0.1/-0.09	0.09/-0.10	0.12/-0.13	

w=1/(σ²F_o²+w₁²*P²+w²*P), where P=(Max(F_o²,0)+2*F_c²)

Table S12. Detailed crystallographic data for PTCDI-Ph at high pressure.

Pressure	0.1 MPa	0.35 GPa	0.49 GPa	0.78 GPa	1.10 GPa	1.47 GPa	1.75 GPa	2.15 GPa	2.50 GPa	2.85 GPa	
CCDC numbers	2253183	2253184	2253185	2253186	2253187	2253188	2253189	2253190	2253191	2253192	
Crystal system	monoclinic										
Space group	<i>P</i> 2 ₁ /c										
<i>a</i> (Å)	16.72(3)	16.773(19)	16.77(2)	16.812(17)	16.759(15)	16.751(10)	16.703(10)	16.688(10)	16.664(12)	16.644(13)	
<i>b</i> (Å)	4.0187(8)	3.8482(6)	3.7945(5)	3.7391(5)	3.6939(4)	3.6491(3)	3.6174(3)	3.5812(3)	3.5410(2)	3.5187(2)	
Unit cell dimensions	<i>c</i> (Å)	18.355(3)	18.186(3)	18.152(4)	18.054(3)	17.998(3)	17.9271(19)	17.8589(18)	17.802(2)	17.695(2)	17.670(3)
α (°)	90	90	90	90	90	90	90	90	90	90	
β (°)	98.55(6)	98.63(6)	98.56(6)	98.49(5)	98.49(4)	98.37(3)	98.33(3)	98.25(3)	98.11(4)	98.14(4)	
γ (°)	90	90	90	90	90	90	90	90	90	90	
Volume (Å ³)		1220(3)	1160.5(14)	1142.2(14)	1122.5(12)	1102.0(10)	1084.1(7)	1067.7(7)	1052.9(7)	1033.7(8)	1024.4(8)
Z/Z'		2/0.5	2/0.5	2/0.5	2/0.5	2/0.5	2/0.5	2/0.5	2/0.5	2/0.5	2/0.5
Calculated density (g/cm ³)		1.477	1.553	1.577	1.605	1.635	1.662	1.688	1.711	1.743	1.759
Absorption (mm ⁻¹)		0.041	0.043	0.043	0.044	0.045	0.046	0.046	0.047	0.048	0.048
F(000)		560.0	560.0	560.0	560.0	560.0	560.0	560.0	560.0	560.0	560.0
Crystal size (mm)		0.14x0.03x0.02	0.14x0.03x0.02								
2θ-range for data collection (°)		5.16 to 34.04	5.206 to 41.442	5.216 to 41.952	5.244 to 42.488	5.26 to 42.476	5.282 to 42.956	5.302 to 42.882	5.32 to 41.222	5.352 to 43.05	5.36 to 40.948
Min/max indices: h, k, l		-8/8,-5/5,-26/25	-13/13,-6/6,-31/30	-13/13,-6/6,-31/30	-13/13,-6/6,-31/30	-13/13,-6/6,-30/30	-13/13,-6/6,-29/30	-13/13,-6/6,-30/29	-13/13,-5/5,-29/30	-14/13,-5/6,-30/29	-14/13,-5/5,-29/28
Reflect. Collected/unique		2508/1236	2678/1537	2652/1522	2604/1490	2540/ 1458	2502/ 1435	2475/ 1414	2381/ 1389	2187/ 1274	2258/ 1280
Data/restrains/parameters		1236/126/190	1537/0/190	1522/0/190	1490/0/190	1458/0/190	1435/0/190	1414/0/190	1389/0/190	1274/12/190	1280/48/190
Goodness-of-fit on F2		0.954	0.866	0.873	0.919	0.978	1.000	0.986	0.997	0.930	0.947
Final R1/wR2 (I>2σ1)		0.0462/0.0735	0.0567/0.1501	0.0429/ 0.0979	0.0655/0.1898	0.0508/0.1264	0.0567/0.1592	0.0530/0.1419	0.0678/0.2020	0.0635/0.1777	0.0619/0.1685
R1/wR2 (all data)		0.1519/ 0.0994	0.1519/ 0.2061	0.1280/ 0.1264	0.1318/0.2385	0.1106/0.1569	0.1054/0.1938	0.0974/0.1697	0.1261/0.2495	0.1324/0.2297	0.1358/0.2319
Largest diff. peak/hole (e.Å ⁻³)		0.08/-0.07	0.16/-0.17	0.12/-0.14	0.15/-0.19	0.12/-0.15	0.16/-0.19	0.17/-0.17	0.22/-0.20	0.18/-0.18	0.18/-0.23

w=1/(σ²F_o²+w₁²*P²+w²*P), where P=(Max(F_o²,0)+2*F_c²)

References

- 1 K. Sato and J. Mizuguchi, *Acta Crystallogr. Sect. E Struct. Reports Online*, 2006, **62**, 5008–5009.
- 2 A. Bondi, *J. Phys. Chem.*, 1964, **68**, 441–451.
- 3 A. Gavezzotti, *Acc. Chem. Res.*, 1994, **27**, 309–314.
- 4 A. Gavezzotti and G. Filippini, *J. Phys. Chem.*, 1994, **98**, 4831–4837.
- 5 T. Langreiter and V. Kahlenberg, *Crystals*, 2015, **5**, 143–153.
- 6 M. Runowski, T. Zheng, P. Woźny and P. Du, *Dalt. Trans.*, 2021, **50**, 14864–14871.
- 7 B. Lorenz, Y. R. Shen and W. B. Holzapfel, *High Press. Res.*, 1994, **12**, 91–99.
- 8 Y. Wang, T. Seto, K. Ishigaki, Y. Uwatoko, G. Xiao, B. Zou, G. Li, Z. Tang, Z. Li and Y. Wang, *Adv. Funct. Mater.*, 2020, **30**, 2001384.
- 9 M. Sójka, M. Runowski, P. Woźny, L. D. Carlos, E. Zych and S. Lis, *J. Mater. Chem. C*, 2021, **9**, 13818–13831.
- 10 J. D. Barnett, S. Block and G. J. Piermarini, *Rev. Sci. Instrum.*, 1973, **44**, 1–9.
- 11 M. A. Antoniak, S. J. Zelewski, R. Oliva, A. Żak, R. Kudrawiec and M. Nyk, *ACS Appl. Nano Mater.*, 2020, **3**, 4209–4217.
- 12 T. Zheng, M. Runowski, N. Stopikowska, M. Skwierczyńska, S. Lis, P. Du and L. Luo, *J. Alloys Compd.*, 2022, **890**, 161830.
- 13 T. Zheng, M. Runowski, P. Rodríguez-Hernández, A. Muñoz, F. J. Manjón, M. Sójka, M. Suta, E. Zych, S. Lis and V. Lavín, *Acta Mater.*, 2022, **231**, 117886.
- 14 M. Runowski, A. Shyichuk, A. Tymiński, T. Grzyb, V. Lavín and S. Lis, *ACS Appl. Mater. Interfaces*, 2018, **10**, 17269–17279.
- 15 A. Katrusiak, *Int. Tables Crystallogr. Vol. H*, 2018, 156–173.